ACS Sustainable Chemistry & Engineering

pubs.acs.org/journal/ascecg

Research Article

Ultrasmooth and Uniform Starch Nanosphere with New Microstructure Formation via Microfluidization−Nanoprecipitation Control

Siyu Yao, Shuohan Ma, Qingqing Zhu, Yu Qin, Wei-ying Ngah, Youming Zuo, Yu Liu, Ximing Zhang, Jinhu Tian, Xiangli Kong, Donghong Liu, and Enbo Xu*

Cite This: *ACS Sustainable Chem. Eng.* 2023, 11, 7475−7488

Read Online

ACCESS | Metrics & More | Article Recommendations | Supporting Information

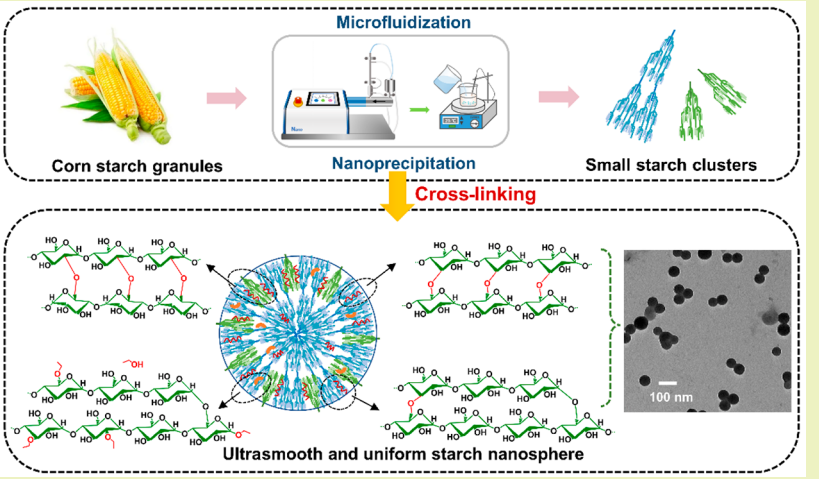

ABSTRACT: Nanostarch has attracted great attention owing to its high biocompatibility, easy availability, low sensitization, small size, and large specific surface area. However, most well-dispersed spherical nanostarches are currently produced under chemical surfactants. Here, we use controllable dynamic high-pressure microfluidization (DHPM) with a nanoprecipitation method to prepare smooth surface and homogeneous starch nanospheres (SNSs). Under the microfluidization condition in a homogenization cycle of ×4 and pressure of 100 MPa, the smallest particle size (67.1 nm) of SNSs with excellent dispersibility (PDI 0.307) was obtained. In addition, after DHPM treating, the crystal structure of starch was damaged. Also, V-type crystallinity was observed after nanoprecipitation, and side chains in starch were cut as performed in an inside-out mode to form small starch clusters. Notably, by mechanical forces, the positions of the OH groups of starch glucan rings were greatly motivated in the spectra of FTIR, ^{1}H NMR, ^{13}C NMR, and XPS. They were cross-linked with each other to form new microstructures of −C−O−C− groups. Furthermore, this should be highlighted for the importance of pressure and homogenization cycle conditions in order to prepare bioresource nanomaterials with well-dispersed properties according to food and nonfood applications like delivery systems.

KEYWORDS: *nanostarch, spherical surface, size distribution, high dispersity, new bound of C−O−C, activated hydroxyl, mechanical impact*

INTRODUCTION

Nanostarch is the bioparticle artificially formed by a glucan chain at nanoscale, which breaks the functional order of native starch with limitations in water solubility, gel stability, dispersibility, porosity, etc.[1] Recently, the controlled structures of nanostarches with diverse morphologies have attracted great attention owing to their various functional properties like high hydrophilicity, stabilization interface,[2] mechanical reinforcement,[3] and antidigestive characteristics[4] as well as good biocompatibility, easy availability, and low sensitization.[5] They have been prepared as spheres, rods, polyhedrons,[6] flakes,[7] and more to meet medicine, cosmetic, environment protection, and food applications.[5] Among them, starch nanospheres (SNSs)

Received: January 31, 2023
Revised: April 6, 2023
Published: May 1, 2023

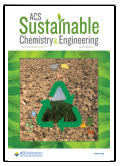

have the most stable topologic surfaces due to tension from the perspective of solid geometry theoretically, which benefits modification or grafting of functional substances used in many aspects, such as nanostarch-reinforced membranes and delivery systems.[4] Compared to inorganic nanoparticles including silica, gold, and iron oxide nanoparticles and some composite nanoparticles like MOF, biopolymeric-based ones are more environmentally friendly and low cost with abundant resources.[8] For example, Lin et al.[9] prepared nanostarch to encapsulate β-carotene. However, those ordered microstructures of inorganic materials give a smooth surface, good regularity, and symmetrical distribution, which show more controllable performances in adsorption, combination, or other binding processes. However, it is always difficult to tailor a spherical nanostarch with an ultracircular surface and uniform size due to the presence of both an interlaced rigid structure (starch crystalline area) and a flexibility structure (starch amorphous area) based on uneven linear and nonlinear polysaccharide chains.

Two strategies are widely used to prepare nanostarch, that is, top-down pathways and bottom-up pathways.[10] The former is a corrosion-like strategy of starch with reagent/bioreagent (e.g., dilute sulfuric acid and hydrochloric acid,[11,12] α-amylase, β-amylase and debranching enzyme[10,13−15]) to remove its amorphous area, which not only generates wastewater but also product residuals as nanostarch with low yield, high crystallinity, and irregular shape. In contrast, the bottom-up pathways especially nanoprecipitation, are known as green, efficient, and controllable methods using recyclable ethanol as an antisolvent to prepare sphere-like nanostarchs (Table S1).[14,15] However, the issue of aggregation and/or agglomeration of SNSs as well as other nanostarches hinders their advantages of large surface area and nanosize effect.[16] The good dispersion of nanostarch in liquid systems is the key to use them. Herein, chemical surfactants were added to modify nanostarch with enhanced repulsion.[17] For example, Mahmoudi Najafi et al.[17] used acetic anhydride and acetic acid to modify corn starch prior to nanoprecipitation, and it was found that the shape of nanostarch performed similar to a spherical morphology with high dispersibility under a low degree of substitution (DS) of 0.23. However, severe conglutination of starch nanoparticles still occurred as DS increased to 2.00 or more.

Dynamic high-pressure microfluidization (DHPM), as a novel physical method, involves combination mechanical actions including high-pressure effect, high-speed impact, and high-frequency vibration as well as instantaneous pressure drops, strong shearing, and hydrodynamic cavitation.[18] During this process, starch suspension is injected into the instrument and divided into multiple streams with strong high-speed impact in the interaction chamber, which could generate starch fragments, i.e., starch nanoparticles, because of the structure collapse by huge forces.[19] Compared with a static high-pressure process, DHPM with special micronic pipelines shows more mechanical forces to efficiently modify the nanostarch structure and properties, and even induce molecular chemical changes by group activation.[20] It is also reported that microfluidization method can not only significantly reduce the particle size and change the molecular structure,[21−23] but can also change the properties of starch granules such as viscosity[24] and solubility.[25] For example, Bitik et al.[23] used microfluidization to treat lentil and chickpea starches, which resulted in lower gelatinization temperatures and apparent viscosities. Kasemwong et al.[26] found that the gelatinization enthalpy of microfluidization-treated cassava starch significantly decreased (from 12 to 3 J/g). However, it has been mainly focused on the structural and functional modifications of starch granules and to the best of our knowledge, there is little research on the formation mechanism and optimization strategy of nanostarch preparation based on the green and reagent-free technology of DHPM so far.

Currently, nanoprecipitation is widely used to prepare SNSs as aforementioned,[15,27−29] and the natural macromolecular chains of starch granules should be gelatinized and degraded into small ones for nucleation and growth to nanostarch. Native starch has a compacted architecture of heterogeneous chain distribution based on amylose, i.e., glucose units connected by α-D-(1,4) glycosidic bonds, and amylopectin, i.e., highly branched glucose chains linked to the main chain by α-D-(1,6) glycosidic bonds.[30] Herein, the sufficient gelatinization of native starch for chain extension is an energy-consuming process with high temperature, and the chain-length distributions are hard to regulate for achieving a uniform size of SNSs. Observation has been given that microfluidization tended to break the starch chain, and notably, amylopectin was easier to degrade than amylose.[31] It could be a pretreatment of nanostarch fabrication followed by nanoprecipitation. The pressure and cycle of dynamic homogenization were relevant to the molecular degradation.[32] However, the effect of DHPM treatment on the specific fracture sites and structural characteristics of starch still needs to be further studied.

To investigate a green method of producing highly homogeneous and dispersive SNSs without surfactant modification, we use DHPM to control the basic structure of starch chains for nanoprecipitation. The strong mechanical force was expected to attack and break starch chains and activate the hydroxyls on their glucopyranose rings. We hypothesized that high pressure might promote tailored starch chain clusters to regularly go through the microchannel and form spherical nanostarch with a smooth surface and uniform size after nanoprecipitation. SNS was designed and efficiently synthesized by DHPM with different pressures and homogenization cycles, which will provide guidance for preparing controllable nanostarch.

MATERIALS AND METHODS

Materials. Native corn starch was provided by Karl Golden (China), without further purification. Phosphate buffer (pH 5.8) was prepared by 0.2 M of sodium dihydrogen phosphate (Macklin, China) and 0.2 M of disodium hydrogen phosphate (Macklin, China) with the ratio of 92 to 8. Absolute ethanol was purchased from Sigma-Aldrich (USA). Potassium bromide (KBr) was provided from Macklin (China). Dimethyl sulfoxide (DMSO)-d6-TMS (1%), potassium iodide, and iodine were purchased from Sigma-Aldrich (USA). Pullulanase (700 U/mL) and isoamylase (1000 U/mL) were purchased from Megazyme (Ireland).

Preparation of SNSs. The starch nanospheres (SNSs) were prepared by DHPM (NanoGenizer, USA) equipped with a diamond cross chamber (F20Y-RT). The corn starch (6 g) was dispersed in 200 mL of phosphate buffer and gelatinized in a boiling bath for 30 min. The solution was cooled to room temperature, and then, it was injected into the microfluidizer under different conditions of pressure (50, 100, 150 MPa) and homogenization cycles (circulation for one time, ×1; circulation for four times, ×4; circulation for seven times, ×7). The microchannel is 75 μm. The sample was cooled by circulating water of 4 °C to keep consistent. After that, the small and uniform sizes of SNSs were formed from the microfluidization-treated

https://doi.org/10.1021/acssuschemeng.3c00575
ACS Sustainable Chem. Eng. 2023, 11, 7475−7488

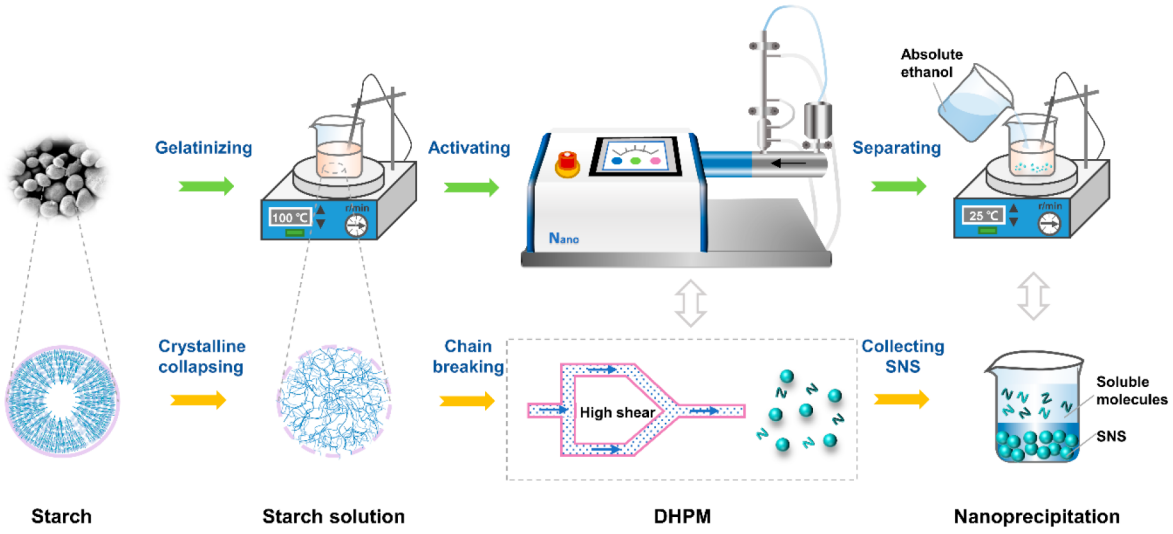

Figure 1. Schematics of starch nanospheres (SNSs) synthesized and controlled by a dynamic high-pressure microfluidization (DHPM)−nanoprecipitation pathway.

solution in nanoprecipitation by adding 300 mL of absolute ethanol with centrifuge at 8000−12000 rpm for several minutes to remove soluble molecules. The nanoprecipitation process was conducted under low-speed homogenization (1500 rpm).[16] The collected supernatants were then freeze-dried at −60 °C for 48−72 h and ground into powder for further tests. The samples were named $SNS_{\times 1-100}$ (with the homogenization cycle of ×1 and pressure of 100 MPa), $SNS_{\times 4-100}$ (with the homogenization cycle of ×4 and pressure of 100 MPa), $SNS_{\times 7-100}$ (with the homogenization cycle of ×7 and pressure of 100 MPa), $SNS_{\times 4-50}$ (with the homogenization cycle of ×4 and pressure of 50 MPa), and $SNS_{\times 4-150}$ (with the homogenization cycle of ×4 and pressure of 150 MPa), respectively.

Dynamic Light Scattering (DLS). The particle diameter distribution of SNS was measured by DLS using a ZET3000-HS Malvern Zetasizer Nano ZS (Malvern, UK) according to the method of Ruan et al.[16] with minor modification. SNS suspension was dispersed by a T 25 Digital ULTRA-TURRAX homogenizer (IKA, Germany) for 15,000 rpm and 2 min, with a concentration of 1 mg of SNS/mL ultrapure water at 25 °C.

Scanning Electron Microscope (SEM). The morphology characterization of SNSs treated by homogenization in a high-pressure microfluidizer with different conditions was performed on a GeminiSEM 300 instrument (Carl Zeiss AG, Germany) operated at an acceleration voltage of 3 kV. The freeze-dried samples were spread on silicon wafers and then sprayed with gold before observation.

Transmission Electron Microscopy (TEM). TEM images were taken using a JEM-1010 instrument (JEOL, Japan) at an acceleration voltage of 80 kV. The SNS suspension was put on carbon-coated copper grids and dried before observation.

X-ray Powder Diffraction (XRD). According to the article of Tang et al.,[33] the crystalline structures of SNSs were determined by a Bruker D8 Advance X-ray powder diffraction analyzer (Bruker, Germany) with a scanning angle (2θ) of 4°−40° using the following parameters: Cu Kα radiation (λ = 0.1542), scan tube voltage (40 kV), current (50 mA), and sweep rate (10°/min). The crystalline pattern of the sample was analyzed by Jade 6.0 software.

Fourier Transform Infrared Spectrometer (FTIR). The chemical structures of SNSs were characterized by a FTIR instrument (Thermo Scientific Nicolet iS50, USA). The sample was mixed with KBr at the ratio of 1:100 and then pressed into tablet. The spectra were scanned 32 times with a wavenumber of 4000−400 cm^{-1}, at a frequency of 4 cm^{-1}. Furthermore, the ratios of IR absorbance at 1047/1022 and 995/1022 cm^{-1} were calculated by OMNIC 8.0 software.

X-ray Photoelectron Spectrum (XPS). The surface chemical compositions of SNSs were conducted using a K-alpha XPS instrument (Thermo, USA) with a spot size of 400 μm at a working voltage of 12 kV and a filament current of 6 mA. The full spectrum scanning energy and narrow spectrum of C and O were 150 eV with a 0.1 eV resolution and 50 eV with a 0.1 eV resolution, respectively.

^{1}H-Nuclear Magnetic Resonance (^{1}H NMR). The distribution of H atoms in SNSs was demonstrated by an AVANCE III nuclear magnetic resonance spectrometer (BRUKER, Switzerland) according to the report of Chen et al.[34] Tetramethylsilane (TMS) was added as the internal standard with 0 ppm. The NS powder (4 mg) was dissolved in 1 mL of DMSO-d6-TMS (1%) with incubation at 60 °C for 10 min to get a transparent solution. The MestReNov software was used to analyzed the spectra.

^{13}C-Nuclear Magnetic Resonance (^{13}C NMR). The chemical characteristic of starch chains was studied by an AVANCE NEO 400WB solid-state nuclear magnetic resonance spectrometer (BRUKER, Switzerland) with a MAS VTN 4 mm probe. The resonance frequency was 100.67 MHz. The spectral width was 4 kHz. The acquisition time was 1.8 ms, and the time domain was 2 s. The contents of C1 (96−106 ppm), C4 (79−84 ppm), and C6 (57−66 ppm) were calculated by MestReNov software.

Chain-Length Distribution. *Iodine Staining Index (ISI).* ISI was used to investigate the iodine binding capacity of amylose and amylopectin as described by Chang et al.,[35] with some modifications. In brief, mother iodine solution was prepared by potassium iodide (2 g) and iodine (0.2 g) and dissolved with deionized water to 100 mL. Then, samples (20 mg) were dispersed in deionized water (20 mL of mother liquor diluted 50 times) for gelatinating at 100 °C for 30 min. Subsequently, 10 mL of the sample solution was mixed with 10 mL of diluted iodine solution to incubate for 30 min at room temperature. The absorbance of the SNS−iodine complex was characterized by a UV-2600 spectrometer instrument (Shimadzu, Kyoto, Japan) in the wavelength range from 400 to 800 nm at the intervals of 1 nm. The absorbance of 557 nm was used to describe the ISI of the SNS−iodine complex.

Size-Exclusion Chromatography (SEC). As previously reported,[33] the amylose chain-length distribution was measured by a LC-20AD SEC system (Shimadzu, Japan) coupled with combination columns of GRAM 1000 and GRAM 100 (Pss, Germany) and a refractive index detector of RID-10A (Shimadzu, Japan). The mobile phase was DMSO/LiBr (5%) at a flow rate of 0.6 mL/min. The sample (4 mg) was dissolved in 5 μL of NaN_3 (0.04 g/mL) and 100 μL of acetic acid (0.1 M, pH 3.5) for gelatinating at 100 °C for 30 min. After the suspension was cooled to room temperature, 6.4 μL of isoamylase (32 U/g) and 2.25 μL of pullulanase (45 U/g) were added into amylopectin at 37 °C for 3 h. Then, the sample freeze-dried overnight was redissolved in a mobile phase solution for SEC analysis. The

https://doi.org/10.1021/acssuschemeng.3c00575
ACS Sustainable Chem. Eng. 2023, 11, 7475−7488

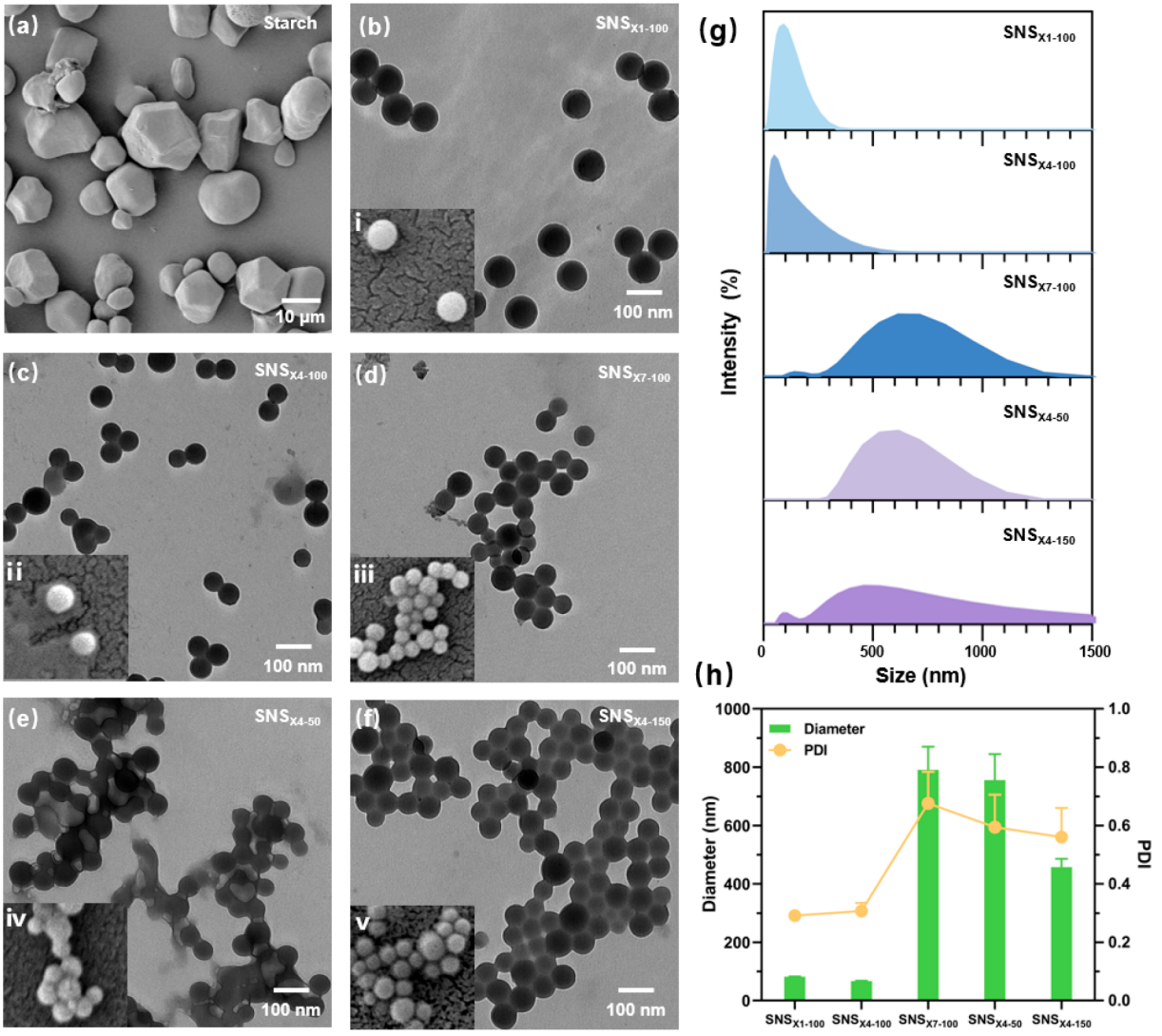

Figure 2. Surface morphology and size distribution of microfluidization−nanoprecipitation starch nanospheres (SNSs). TEM images of (a) native starch and (b−f) nanostarch, prepared via dynamic high-pressure microfluidization in different conditions of pressure and cycle: (b) ×1, 100 MPa, i.e., SNS_{x1-100}; (c) ×4, 100 MPa, i.e., SNS_{x4-100}; (d) ×7, 100 MPa, i.e., SNS_{x7-100}; (e) ×4, 50 MPa, i.e., SNS_{x4-50}; and (f) ×4, 150 MPa, i.e., SNS_{x4-150}. SEM images of (i−v) nanostarch. (i) SNS_{x1-100}, (ii) SNS_{x4-100}, (iii) SNS_{x7-100}, (iv) SNS_{x4-50}, and (v) SNS_{x4-150}. (g) Size distributions and (h) average diameters and polydispersity indexes (PDI) of SNSs.

amylose content (AC) and branching degree (BD) were calculated according to eqs 1 and 2. AC is related to the ratio of the area under the curve (AUC) of DP 100−20000 of the SEC weight CLDs to the area under the curve of DP 1−20000, $N_{de}(x)$ is the number distribution of chains.

$$AC(\%) = \frac{AUC_{DP100-20000}}{AUC_{DP1-100} + AUC_{DP100-20000}} \times 100 \quad (1)$$

$$BD(\%) = \frac{1}{N_{de}(x)} \times 100 \quad (2)$$

High-Performance Anion-Exchange Chromatography (HPAEC). The amylopectin chain-length distribution of SNSs was analyzed by a HPAEC system (Thermo Fisher ICS-5000 Plus, USA) equipped with a pulsed amperometric detector, BioLC gradient pump, and column (Carbo-Pac-100 column) according to the document of Kong et al.[36] The mobile phase was a mixture of NaOH (eluent A,150 mM) and NaOAc (eluent B, 1 M) at a rate of 1 mL/min. In the initial 1.3 min, eluent A was decreased to 93% linearly, then 82% in 10 min, 78% in 19 min, 50% in 111 min, and 93% in 113 min, respectively. The sample (9 mg) was dispersed by 450 μL of DMSO for gelatinating at 100 °C for 2 h. Then, the solution was cooled to room temperature and diluted with 1050 μL of deionized water and 1500 μL of sodium acetate buffer (0.1 M, pH 4.5). Subsequently, 1 μL of pullulanase (700 U/mL) and 1 μL of isoamylase (1000 U/mL) were added to debranch amylopectin at room temperature overnight with constant stirring. The solution was centrifuged at 8000 rpm for 10 min and filtered through 0.45 μL of membrane before injection into the system. The amylopectin chain-length distribution was recorded and corrected by Version 6.8 Chromeleon software.

RESULTS AND DISCUSSION

Uniform Size and Spherical Morphology. The schematics of the starch nanoparticles, i.e., SNSs, are displayed in Figure 1 using the combined method of the microfluidization−precipitation process. Microfluidization was conducted by a DHPM instrument where a gelatinized starch solution was violently collided and oscillated due to high-velocity impact, powerful shearing, instantaneous pressure dropping, and even cavitation force attacking.[20] It resulted in

https://doi.org/10.1021/acssuschemeng.3c00575
ACS Sustainable Chem. Eng. 2023, 11, 7475−7488

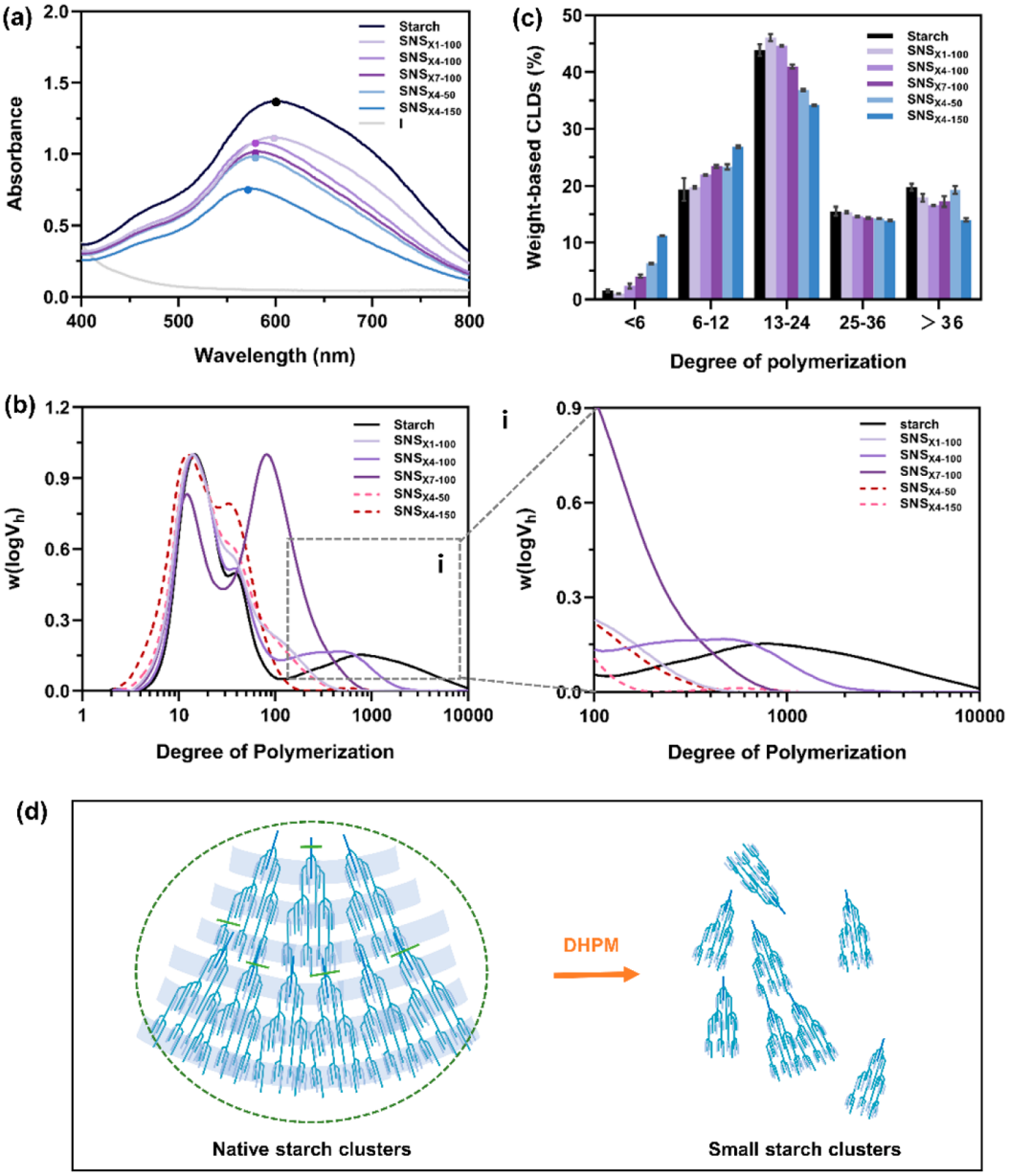

Figure 3. Basic structure of chain-length distribution (CLD) of microfluidization−nanoprecipitation starch nanosphere (SNS). (a) Amylose iodine complex of native starch and nanostarch samples (×1, 100 MPa, i.e., $SNS_{×1-100}$; ×4, 100 MPa, i.e., $SNS_{×4-100}$; ×7, 100 MPa, i.e., $SNS_{×7-100}$; ×4, 50 MPa, i.e., $SNS_{×4-50}$; ×4, 150 MPa, i.e., $SNS_{×4-150}$). (b) Weight distribution [w (log V_h)] of both amylopectin and amylose chains of SNSs from the degree of polymerization (DP) by SEC analysis. (i) Magnified w (log V_h) at DP value of amylose chains of SNS. (c) Chain-length profiles of amylopectin of SNSs obtained by HPAEC analysis. (d) Proposed structural units of tailored starch clusters in SNSs.

the breaking of main chains and part of side chains in starch, accompanied by structural change and intramolecular/intermolecular bond formation (see below). The DHPM-tailored starch clusters with activated groups recombined to SNSs with morphological screening and new cross-linking structures via nanoprecipitation.

The surface morphologies of SNSs are illustrated by TEM and SEM images in Figure 2a−f (i−v) and Figure S1. Native starch showed an irregular and polygonal shape at the microscale (Figure 2a). Compared with pure nanoprecipitation-treated nanostarch (Table S1), almost all SNSs in this study showed much rounder and smoother surfaces that were successfully prepared under different microfluidization conditions of cycle and pressure (×1−100 MPa, ×4−100 MPa, ×7−100 MPa, and ×4−150 MPa except for ×4−50 MPa). As the homogenization cycle of DHPM treatment increased, spherical starch nanoparticles had no change on their smooth surface but were gradually decreased in size. You's work[37] used lotus seed starch slurry treated by microfluidization, and they also found that the particle average diameter decreased from 11.93 to 10.80 μm in the pressure of 40 MPa and cycle of ×5. In order to get nanoscale starch spheres, here the intermolecular hydrogen bonds were weakened by initial gelatinization, and the crystal structures of large chain clusters were broken down followed by ethanol precipitation.[38,39] Interestingly, SNSs showed excellent dispersal ability with the preparing conditions at 1 and 4 times of microfluidic circulation but sharply reduced at 7 times when pressure was

https://doi.org/10.1021/acssuschemeng.3c00575
ACS Sustainable Chem. Eng. 2023, 11, 7475−7488

stable at 100 MPa. It may be related to the integrated mechanical forces which should be controlled at an appropriate range, and we speculated that excessive activation of starch chains led to SNS agglomeration.[7,40−42] A similar phenomenon of SNS agglomeration was observed for samples treated at high pressure of 150 MPa but only microfluidic cycling for 4 times. Furthermore, it is noted that only a quasi-circular shape of microfluidization−precipitation nanostarch (like starch gel) was obtained when pressure was only 50 MPa (Figure 2e), indicating that enough mechanical action was necessary for forming the embryonic forms of stable spheres of nanostarch.

To understand the trends of size alternation with treating conditions, the details of size distributions and polydispersity indexes (PDI) of SNSs are detected and shown in Figure 2g and h. The average diameters of $SNS_{\times1-100}$, $SNS_{\times4-100}$, $SNS_{\times7-100}$, $SNS_{\times4-50}$, and $SNS_{\times4-150}$ were 81.7, 67.1, 790.8, 756.1, and 457.6 nm, respectively. As the microfluidic cycle increased from ×1 to ×7, the SNS size first and slightly decreased but dramatically increased about 8 folds probably due to aggregation. Herein, the particle size of $SNS_{\times1-100}$, $SNS_{\times4-100}$, and $SNS_{\times4-50}$ had only one peak in DLS patterns, which was attributed to the highly dispersed particles of $SNS_{\times1-100}$, $SNS_{\times4-100}$, and aggregated particles of $SNS_{\times4-50}$, respectively (Figure 2g), while the particle sizes of $SNS_{\times7-100}$ and $SNS_{\times4-150}$ had one huge peak in PLS patterns with a negligible micropeak (i.e., scattered SNS which could be observed in Figure 2d, f). Compared with samples microfluidization-treated under 100 MPa, the average sizes of SNS samples at 50 and 150 MPa all increased several times under the same microfluidic cycle (Figure 2h). This result is similar to that of SEM/TEM images of SNSs. The cycle and pressure of microfluidization had a significant influence on the material particle diameter as previous reported.[21] Notably, the diameter peak shapes of $SNS_{\times4-50}$ (near sharp) and $SNS_{\times4-150}$ (broad) were totally different while both showed a poor dispersion performance. This may be because the mechanical forces under the pressure of 50 MPa were too weak to shear and compact starch chains for SNS formation, whereas that under the pressure of 150 MPa was too strong for gelatinized starch to form and keep single SNSs in the presence and release of instantaneous high pressure. Besides, with the pressure increased, the number of small particles increased, possibly resulting in the intensifying of the van der Waals force and electrostatic attraction on SNS surfaces with secondary particles forming.[43] The aggregation of $SNS_{\times7-100}$ also occurred probably due to water absorption and deformation.[7] Therefore, the optimal synthesized process of SNSs was pressure of 100 MPa and a microfluidic cycle of ×4 in this study.

Identification of Chain-Length Distribution. To illustrate the structures of SNSs, the basic compositions of starch chain-length distribution (CLD) including amylose and amylopectin were identified (Figure 3). It is known that helical complexes could be formed between iodine and amylose/amylopectin long chains. The absorption spectra of SNS−iodine(I) complexes are presented in Figure 3a. Compared with native starch, the absorbances of SNSs at 400−800 nm were all decreased, indicating the remarkable action of the microfluidization and nanoprecipitation process to crack and separate starch chains. The blue shift of the absorption peak occurred from 596 nm of the native starch to 572 nm of nanostarch, especially under high pressure of microfluidization (150 MPa). The iodine staining index (ISI) is positively related to the average chain length of SNSs. The absorbance of 557 nm is used to describe the ISI of the SNS−I complex, and the absorbances at 460 and 570 nm are characterized for the shorter and longer chains, respectively.[44] As the homogenization cycle increased from ×1 to ×7, the absorbance value at 557 nm decreased from 0.9608 to 0.9412, and the best absorbance peak shifted from 596 to 583 nm, implying that increasing microfluidic circulation was beneficial to cut starch chains (Table 1). Moreover, the I-adsorption performances of

Table 1. Special Absorption of Native Starch and Nanostarch in Ultraviolet-Visible Spectral

Sample	λ = 460 nm	λ = 570 nm	λ = 557 nm (ISI)
Starch	0.5838	1.271	1.164
$SNS_{\times1-100}$	0.4754	1.0487	0.9608
$SNS_{\times4-100}$	0.4779	1.0574	0.9893
$SNS_{\times7-100}$	0.4548	0.9995	0.9412
$SNS_{\times4-50}$	0.4455	0.9728	0.9204

SNSs treated through microfluidic pressures of 50, 100, and 150 MPa were significantly different. In all samples, $SNS_{\times4-150}$ showed the minimum absorption with the lowest CLDs due to high pressure with a strong impact on the crystalline regions of starch, and the proportion of amylose in SNSs was decreased while those branched chains in starch clusters were increased (see below).[45]

To further explore the CLDs of SNS, amylopectin (DP < 100) and amylose (DP > 100) detection are shown in Figure 3b and c. Compared to native starch, long chains (DP > 1000) of SNSs were significantly shortened. Amylose content (AC) containing DP from 100 to 10000 was calculated and is listed in Table S2; AC of SNS decreased to some extent, especially under the condition of ×4, 150 MPa. AC decreased from 23.599% to 1.653%, indicating the breaking ability of mechanical forces on α-D-(1,4) glycosidic bonds of long chains. Notably, as microfluidic circulation increased, AC gradually raised from 8.668% to 27.049%, contrary to the data of ISI. It was speculated that DHPM was sensitive to amylose chains, and these free long chains were degraded under strong forces. The maximum absorption peak in ISI occurred to a blue shift as microfluidic circulation increased. However, the O−H bonds in starch chains were activated resulting in molecular chain crossing between/within clusters (details see below). Besides, during the SEC method, crossing chains (which could not form complexes with iodine) were not debranched before detecting, leading to the detection of higher AC values. Moreover, the branching degree (BD) of all SNS samples almost rose from the perspective of the overall trend, but it decreased from DP 1−100 and increased from DP 100−10000, which was related to the degradation of amylose and crossing chains, respectively (Table S2).

The weight-based distributions of debranched amylopectin of SNSs are shown in Figure 3c. Amylopectin is divided into five regions: B3 chain (DP > 36), B2 chain (DP 25−36), B1 chain (DP 13−24), A chain (DP 6−12), and ultrashort chain (DP < 6).[46] Compared with native starch, the proportion of five regions of nanostarch changed after microfluidization treatment. Under the conditions of ×1−100 MPa, the content of B3 chains and B2 chains of SNSs reduced, from 19.743% to 17.920% and 15.487% to 15.320%, respectively, while B1 chains and A chains raised from 43.843% to 46.047% and 19.323% to 19.731%, respectively, due to the degradation of

https://doi.org/10.1021/acssuschemeng.3c00575
ACS Sustainable Chem. Eng. 2023, 11, 7475−7488

large starch clusters (Table S3). However, the B1 chains gradually reduced and transformed to A chains and ultrashort chains as the microfluidic circulation increased. We guessed that mechanical forces in the DHPM process acted on the longer main (DP 100−10,000) and submain chains (i.e., B3 chain and B2 chain), then on side chain (i.e., B1 chain), with the mechanism of starch chain attacking in inside-out mode, which is similar to the report of Chen et al.[47] Furthermore, $SNS_{\times4-150}$ with the highest pressure had a higher content of A chains and ultrashort chains but lower contents of B3, B2, and B1 chains.

Overall, the stronger the mechanical forces of DHPM on a starch molecule are, the shorter are the chains in CLDs of SNS samples. Long chains are preferentially degraded resulting in the formation of small clusters. The supposed DHPM-induced degradation mechanism is performed in Figure 3d. Wei et al.[48] reported that mechanical forces preferentially disrupted larger molecules and confirmed the breakdown of the α-1,4-glycosidic bonds rather than α-1,6-glycosidic bonds among the amylopectin with the midpoint scission mechanism.

Changes in Crystals and Long-/Short-Range Orders. To analyze the influence of microfluidization on the crystal structures of SNSs, the long-range orders of crystals according to XRD patterns of samples are presented in Figure 4a. The mechanical forces of DHPM showed a great impact on gelatinized starch gel, which may lead to the collapse of crystal structure for SNS formation. The native starch had an A-type X-ray pattern with major peaks (2θ) of 15°, 17°, 18°, and 23°, respectively.[49] While SNS samples all had two obvious diffraction peaks at 2θ of 13° and 20°, indicating that a V-type crystalline structure was generated.[50] This was probably due to the presence of a single helix structure embedded with ethanol, which was caused by the loose A-type crystal structure after starch gelatinization and mechanical disruption.[51] It was also interesting that these new peaks disappeared when microfluidic pressure was enhanced up to 150 MPa, but all peaks of $SNS_{\times4-150}$ shifted 0.5° to the right, which showed the damage and remodeling effects of high pressure on crystal structure.

As shown in Table 2, compared with native starch with relative crystallinity of 22.51%, the SNS samples dramatically decreased in their crystallinities. At microfluidic cycles of ×1, ×4, and ×7, the relative crystallinity was 5.92%−8.65%. The appropriate mechanical action may benefit the recrystallization of tailored starch chains assisted by antisolvent-induced separation. At increasing pressure from 50 to 150 MPa, the relative crystallinity decreased from 9.64% to 7.02%. It indicated that pressure strength also had effects on the crystallinity reduction of SNSs. Based on these results, we tentatively speculated that DHPM could destroy the amorphous regions and crystalline regions of starch together, leading to the degradation of amylopectin and amylose.[52] When mechanical action was strengthened by increasing microfluidic circulation as pressure stable under 100 MPa, hydrogen bonds between molecules were broken, and crystalline regions swelled and rearranged resulting in a decrease of relative crystallinity.[45] This result was similar to the previous report of Wang et al.[7]

The short-range orders of SNS crystals were detected by FTIR,[53] which is observed in Figure 4b. The smooth and broad band at 3600−3300 cm^{-1} of native starch correspondsto the vibration of O−H.[54] Among them, 3600−3500 and 3500−3300 cm^{-1} represent free hydroxyl, intramolecular, and intermolecular hydrogen, respectively.[55] Surprisingly, the absorption peak strength at these positions decreased and

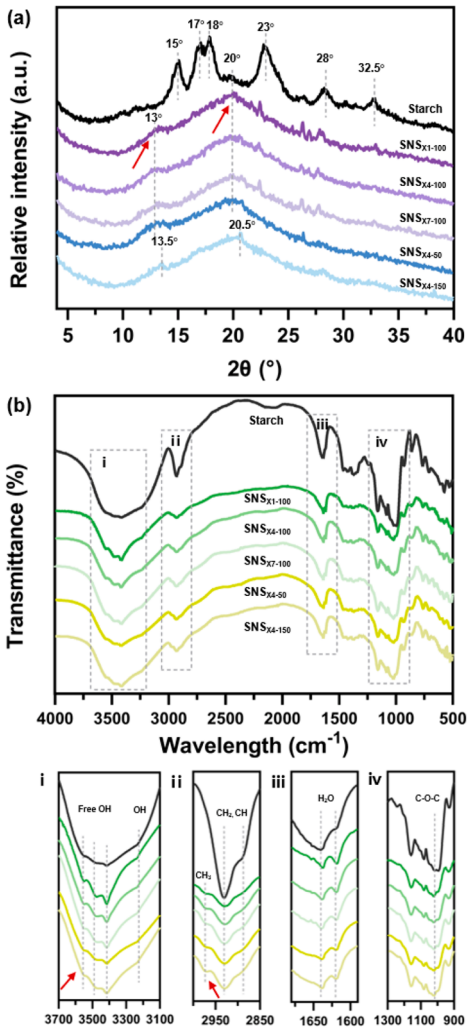

Figure 4. Crystalline structure and chemical group of microfluidization−nanoprecipitation starch nanospheres (SNSs). (a) XRD patterns and (b) FTIR spectra of native starch and nanostarch samples (×1, 100 MPa, i.e., $SNS_{\times1-100}$; ×4, 100 MPa, i.e., $SNS_{\times4-100}$; ×7, 100 MPa, i.e., $SNS_{\times7-100}$; ×4, 50 MPa, i.e., $SNS_{\times4-50}$; ×4, 150 MPa, i.e., $SNS_{\times4-150}$), magnified FTIR spectra at (i) 3700−3100 cm^{-1}, (ii) 3000−2850 cm^{-1}, (iii) 1650−1600 cm^{-1}, and (iv) 1300−900 cm^{-1} of SNS.

Table 2. Crystal and Chain Helix Characteristics of Native Starch and Nanostarch Samples[a]

Sample	Crystallinity (%)	Double helices content (%)	Single helices content (%)	DD	DO
Starch	22.51	62.77	14.36	0.81	1.12
$SNS_{\times1-100}$	5.92	58.76	12.54	0.73	0.88
$SNS_{\times4-100}$	8.65	59.24	12.61	0.78	0.92
$SNS_{\times7-100}$	8.44	57.52	12.39	0.73	0.94
$SNS_{\times4-50}$	9.64	58.03	12.44	0.74	0.91
$SNS_{\times4-150}$	7.02	59.71	13.70	0.77	0.96

[a]Crystallinity was calculated from XRD. Double helices content and single helices content were calculated from ^{13}C NMR. Degree of double helices (DD) and degree of order (DO) were calculated from FTIR.

https://doi.org/10.1021/acssuschemeng.3c00575
ACS Sustainable Chem. Eng. 2023, 11, 7475−7488

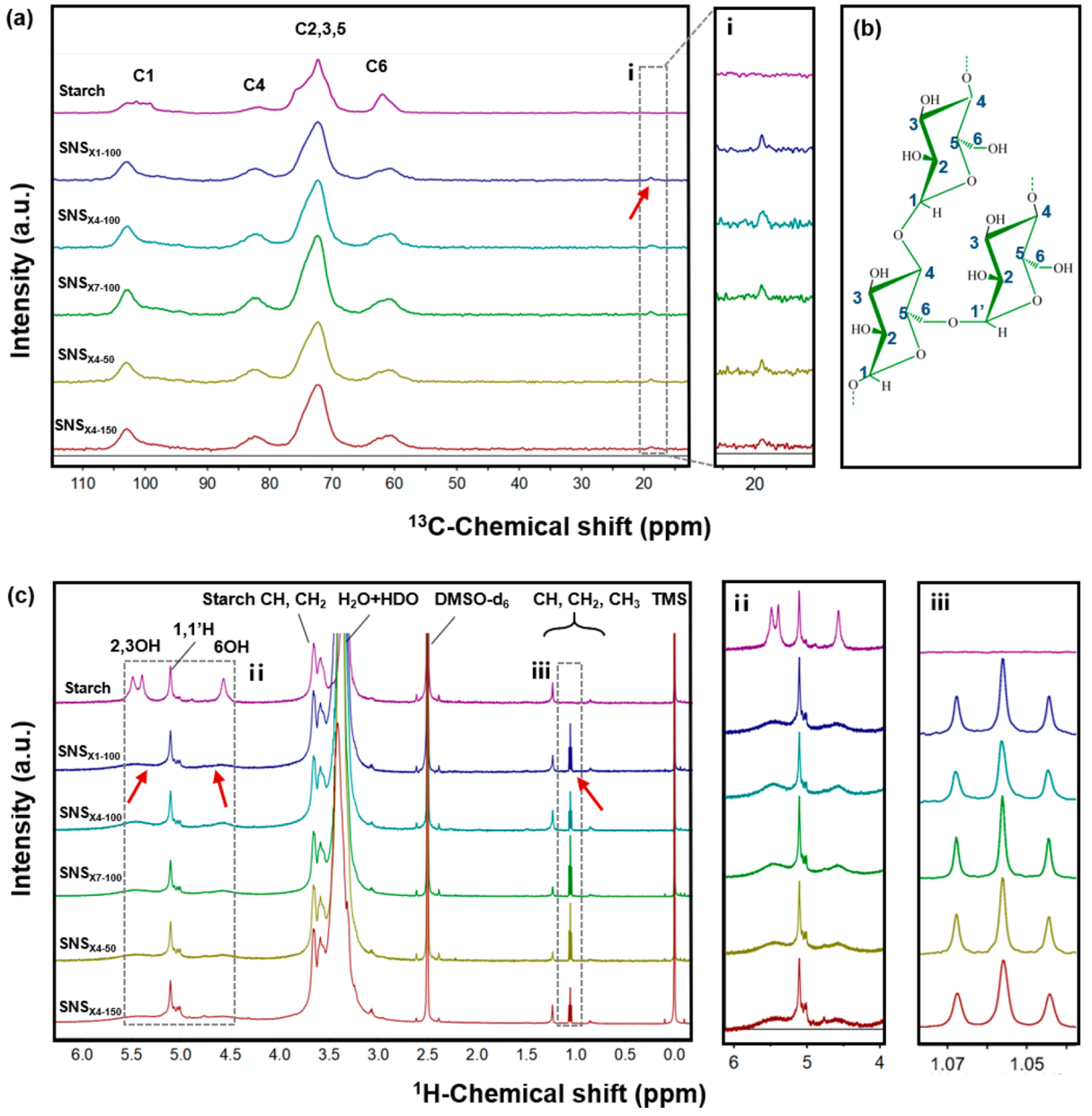

Figure 5. Molecular structure characteristics of microfluidization−nanoprecipitation starch nanosphere (SNS). (a) ^{13}C NMR, magnified peak at (i) 25−15 ppm of SNS. (b) Marked starch structures of C1−C6 in glucopyranose rings. (c) ^{1}H NMR of native starch and nanostarch samples (×1, 100 MPa, i.e., SNS$_{×1-100}$; ×4, 100 MPa, i.e., SNS$_{×4-100}$; ×7, 100 MPa, i.e., SNS$_{×7-100}$; ×4, 50 MPa, i.e., SNS$_{×4-50}$; ×4, 150 MPa, i.e., SNS$_{×4-150}$), magnified peak at (ii) 6−4 and (iii) 1.1−1.0 ppm of SNSs.

changed to a sharp "multipeak" for SNSs in comparison with the native one (Figure 4b (i)), indicating the change of hydrogen bond interactions after microfluidization−nanoprecipitation treatments. It was worth noting that as the microfluidic cycle increased, the absorption peak at 3600−3300 cm^{-1} changed to smoother. Among different pressure conditions, the SNS sample in 100 MPa was observed with sharper peaks (similar to the results of relative crystallinity), showing effects of mechanical forces on the intramolecular and intermolecular hydrogen. The peak at 2930 cm^{-1} is ascribed to the asymmetric C−H stretching vibration.[50] As shown in Figure 4b (ii), a new peak occurred at 2970 cm^{-1}, indicating the generation of a new C−H stretching vibration. Here, 1653 cm^{-1} is assigned to the complex bending vibration of O−H of water absorbed in the amorphous area.[56] DHPM dramatically reduced the bound water holding capacity of SNS after lyophilization (Figure 4b (iii)), but it is hard to define this without further structural analyses (see below). Furthermore, the band at 1156 cm^{-1} is related to C−O, C−C, and C−OH stretching.[56] In particular, the fingerprint region (800−1200 cm^{-1}) is associated with the helical structure of native starch and SNSs (Figure 4b (iv)).[57] Generally, the absorbance at 1047/1022 is linked to the ratio of ordered structure to amorphous structure, which is defined as the degree of order (DO),[58] and 995/1022 cm^{-1} shows the degree of double helices (DD).[59] As shown in Table 2, DD and DO of SNS samples were lower than native starch, indicating the destruction of short-range orders of crystals.

Molecular Structure Modification. As aforementioned, we found a significant decrease in hydroxyl groups in SNSs and

https://doi.org/10.1021/acssuschemeng.3c00575
ACS Sustainable Chem. Eng. 2023, 11, 7475−7488

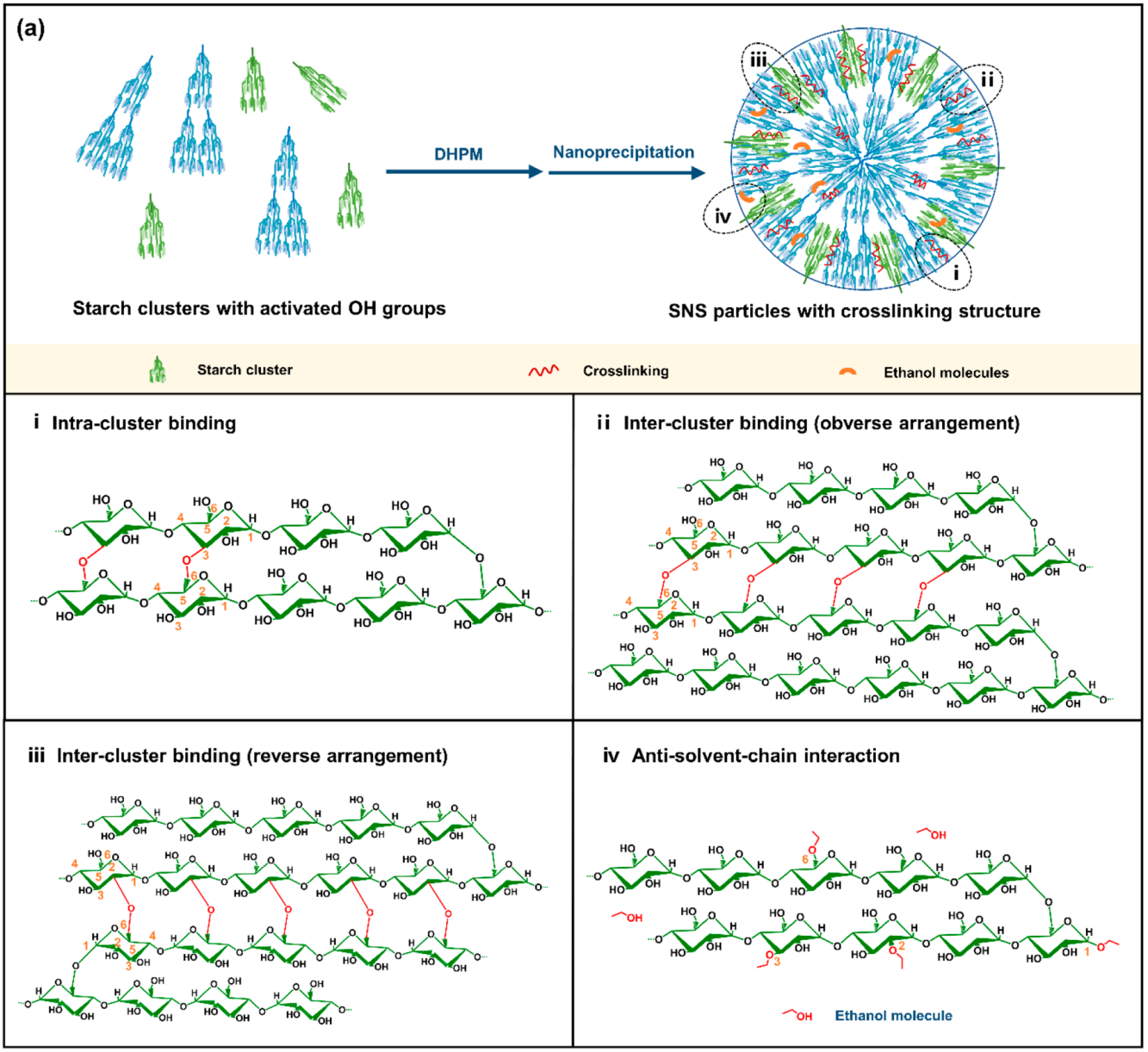

Figure 6. Proposed mechanism for the cross-linking of starch chain inside SNSs by the microfluidization−nanoprecipitation pathway. (a) SNS particle with cross-linking structure: (i) intracluster binding, (ii) intercluster binding of obverse arrangement, (iii) intercluster binding of reverse arrangement, and (iv) antisolvent-chain interaction.

new C−H and C−O−C bonds as well as crystal peaks were formed in the FTIR/XRD spectra of these nanostarches, with BD in the DP 100−10,000 significantly increased. In order to further reveal the new bond positions and nanostructure compositions of SNSs, ^{13}C NMR, ^{1}H NMR, and XPS were used to characterize the molecular structures of SNSs.

As shown in Figure 5a, the carbon chemical shift could be respectively divided into four regions: 100−110 ppm (C1 region), 80−85 (C4 region), 71−74 ppm (C2, C3, C5 region), and 58−63 ppm (C6 region).[60] The C1 region is related to the crystallinity type and scope.[61] The native starch shows three typical peaks related to the three glucose residues in its spiral symmetric arrangement of 99.5, 100.4, and 101.5 ppm and one amorphous peak of 102.9 ppm, which is classified as A-type crystalline.[62] After gelatinization and the microfluidization−nanoprecipitation process, the three typical crystal peaks almost fully disappeared, leaving only one amorphous peak which is from V-amylose.[63] This result was consistent with XRD patterns. Moreover, the resonances of C6 peaks of SNS samples moved downfield from 62.0 to 60.5 ppm and were all broader in comparison with that of native starch. The broader NMR resonance was attributed to the less short-range order.[63] In addition, the result was explained as the previous report of Veregin et al.[64] that the NMR line width of C6 resonance was due to the existence of many conformations for the C6 hydroxyl, which may be in some dynamic exchange state. There were changes of line width and resolution in C2, 3, 5 spectral regions. Native starch exhibits one peak and two shoulder peaks, which are assigned as follows: 75.5, 73.0, and 69.5 ppm, while the C2, 3, 5 spectral regions of all SNS samples were dominated by a broad and signal centered at 73.0 ppm. The result was related to the decrease of hydration and

https://doi.org/10.1021/acssuschemeng.3c00575
ACS Sustainable Chem. Eng. 2023, 11, 7475−7488

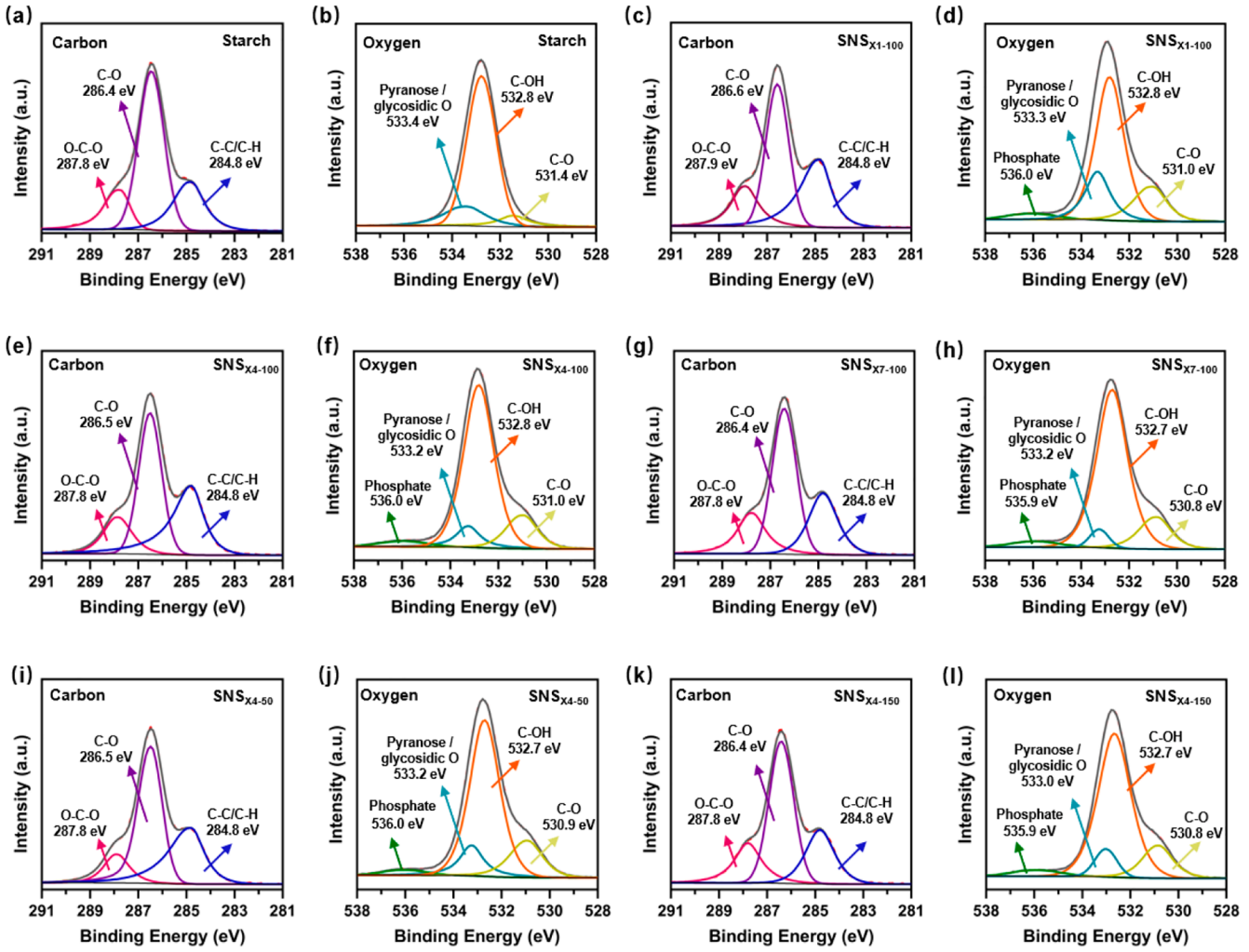

Figure 7. Surface elements of microfluidization−nanoprecipitation starch nanospheres (SNSs). (a) C 1s and (b) O 1s in XPS patterns of native starch. (c, e, g, i, k) C 1s and (d, f, h, j, l) O 1s in XPS patterns of nanostarch samples (×1, 100 MPa, i.e., $SNS_{×1-100}$; ×4, 100 MPa, i.e., $SNS_{×4-100}$; ×7, 100 MPa, i.e., $SNS_{×7-100}$; ×4, 50 MPa, i.e., $SNS_{×4-50}$; ×4, 150 MPa, i.e., $SNS_{×4-150}$).

crystallinity.[63] C2, C3, and C5 regions and the C6 region could provide information about double and single helixes,[61,65] respectively (Table 2). The changes of the contents of starch chain helices seemed not significant, and the helical structure was still unclear. It was speculated that the natural double helices in starch crystal regions had been destroyed, and a novel double/single helix may be formed but not crystallized orderly, leading to decreased crystallinity with a changed type of SNS. Moreover, it must be noted that compared to native starch, the new resonance of SNSs in 19−20 ppm emerged (Figure 5a (i)), which was assigned to C−H,[34] except for starch C1−6 regions.

To further investigate the change of H protons in SNSs, the liquid ^{1}H NMR spectra of native starch and SNS samples were measured in DMSO-d_6. The results are shown in Figure 5c; the peak in 0 ppm was related to tetramethylsilane, which helped to accurately correct the signal position of H protons. The spectra clearly display the chemical shifts of H at 5.11 ppm (H1) and 3−4 ppm (H2, 3, 4, 5, 6). Meanwhile, the peaks of −OH were assigned to 5.51, 5.40 (OH3, OH2), and 4.58 ppm (OH6), respectively,[34] with the peaks of H_2O and HDO related to 3.33 ppm. In accordance with FTIR results, the signals of OH2, OH3, OH6, and H_2O of SNS samples decreased synchronously in comparation with native starch (Table S4). It proved that the hydroxyl bonds in C2, C3, and C6 were all activated by strong mechanical forces and interacted with each other. The cross-linking mechanism was proposed between local starch clusters (1) intracluster binding (Figure 6a (i)), (2) intercluster binding (Figure 6a (ii, iii)), and (3) antisolvent-chain interaction (Figure 6a (iv)). First, from a perspective of chain extension and steric hindrance, the microfluidization-activated OH6 in main chains (i.e., B3 chain) and dominant B2 chains may bind to activated OH3 in their side chains (B1 and A chains) for an aligned structure, with C−O−C formation and H_2O removal. Then nonintrachain binding would occur between activated chains in different tailored clusters or free amylose. Due to spherical but not prismatic/rhombic structures of total SNSs, we conjectured that they may be present in reverse arrangement for the stable binding of OH6 and OH2 as well as obverse arrangement for the binding of OH6 and OH3. Furthermore, a new signal at 1.00 ppm in the ^{1}H NMR of SNS was obtained and characterized as the new bond of C−H (Figure 5c (iii)), relative to the new peaks in ^{13}C NMR (19−20 ppm) and FTIR (2970 cm^{-1}), which was assigned to the $-CH_3$ of ethanol. As the previous reports, a small ethanol molecule could enter the

https://doi.org/10.1021/acssuschemeng.3c00575
ACS Sustainable Chem. Eng. 2023, 11, 7475−7488

spiral cavity of amylose to form V-typed complexes with hydrophobic interactions.[66,67] However, in this work, we considered the combination of the ethanol molecule to the activated −OH groups and to the reducing end of starch chains (occurred in DHPM) during the nanoprecipitation process. This phenomenon has not been reported by other studies yet.

To further clarify the cross-linking mechanism and surface structure with the new position of C−H, XPS was used to measure the chemical environment of oxygen (O) and carbon (C) atoms (Figure 7). XPS is a useful tool to explore surface chemical changes with the analysis depth of 6−8 nm. The general XPS spectra of native starch and SNS samples are displayed in Figure S2. The peaks around 532 and 268 eV correspond to oxygen and carbon atoms, respectively. The elemental surface composition and the ratios of O to C are presented in Table S5. The O/C ratio of native starch was equal to 0.67, while all SNSs of that increased even to 0.88, which may be due to the exposure of −OH groups. The C 1s and O 1s peaks of native starch and SNS samples were deconvoluted into several peaks, which are presented in Figure 7. In C 1s spectra, the peaks of SNSs around 284.8, 286.4, and 287.8 eV correspond to the C of C−C/C−H (carbon atoms bonded with carbon or hydrogen atom), C−O (carbon atoms linked with a single oxygen atom), and O−C−O (carbon atoms bonded to two oxygen atoms). In O 1s spectra, the peaks of 531.4, 532.8, and 533.4 eV are related to C−O (oxygen atoms bonded with two carbon atoms), C−O−H (oxygen atom bonded to one carbon atom and one hydrogen atom), and glycosidic O (oxygen atoms in glycosidic ring), respectively. As shown in Table S6, after microfluidization−nanoprecipitation treatment, the ratio of C−C/C−H to C−O for C 1s was higher than native starch, because the −OH groups of starch chains had been activated, and ethanol molecules had been successful grafted on the SNS surfaces. For O 1s, the intensity of C−O peak was higher, and the C−O−H peak was lower in comparation to native starch. As previously mentioned, three chemical reactions occurred in the whole system: (1) starch chain breakage, (2) intracluster and intercluster cross-linking, and (3) grafting of ethanol molecular. Among them, chain breakage caused the fracture of the C−O−C bond and the formation of the C−O−H bond. Cross-linking and grafting chemical modifications resulted in the reduction of the C−O−H bond and the formation of a C−O−C bond. Herein, the effect of hydroxyl groups generated by α-1,4-glycosidic bond breaking was less than that of ethanol grafting and that of starch chain cross-linking.

According to the results above, the formation mechanism of uniform and good spherical SNSs could be summarized as follows. First, the starch chains were unfolded with sufficient gelatinization. Then, the starch solution was violently collided and oscillated due to the violent mechanical forces of DHPM, which led to the generation of activated −OH groups and the break of main chains and some side chains for forming the SNS units of small clusters. During the collision in the cavity, cross-linking occurred in interclusters and intraclusters, with the formation of C−O−C bonds to form a smooth spherical morphology (Figure S3). After that, ethanol was added to generate an unbalanced interaction including surface tension changes, flow, and diffusion,[27,68,69] and the free activated −OH groups were continuously crashed and cross-linked, which explained that the intensity of the −OH peak in ^{1}H NMR was slightly decreased with DHPM treatment and dramatically reduced after nanoprecipitation. Besides, after nanoprecipitation, the particle size distribution of SNSs was better dispersed compared to the microfluidization sample without nanoprecipitation, showing the separation ability of ethanol (Figure S3a, b). Overall, the proposed mechanism for cross-linking of starch chains in SNSs is shown in Figure 6.

CONCLUSIONS

In this work, starch nanospheres, i.e., SNSs, were successfully prepared with controllable sizes, high dispersibility, and smooth spherical morphology through green processes of gelatinization, microfluidization, and nanoprecipitation combining thermal and mechanical actions. The condition of microfluidization (here using DHPM) was obtained to form SNS (67.1−81.7 nm) with the good dispersibility (PDI 0.291−0.307). The starch chain distribution of the CLD model was established and correlated with SNS structures, and the transfer trend of the long chain proportion to the short one in starch clusters illustrated the potential mechanism of DHPM impacting for the generation of small clusters as the structural units of SNSs. The crystal structure based on the change of starch chains showed an inside-out mode, and V-type crystallinity was observed after nanoprecipitation, which was beneficial for functional guest embedment. FTIR, ^{1}H NMR, ^{13}C NMR, and XPS analyses indicated that the −OH groups of starch were activated by DHPM, and a new bond of C−O−C was obtained probably due to (1) the cross-linking of activated −OH groups between C2/C3 and C6 intra/interclusters and 2) the combination of antisolvent ethanol to these −OH groups. The later conjecture could also explain the new C−H response in SNSs, which may be due to the generation of a reducing end on C1 from DHPM broken starch chains.

ASSOCIATED CONTENT

Supporting Information

The Supporting Information is available free of charge at https://pubs.acs.org/doi/10.1021/acssuschemeng.3c00575.

Nanostarch with different morphologies and crystalline types (Table S1). Circularity of SNSs and nanostarch previously reported (Figure S1). Chain-length distributions (CLDs) of amylose in nanostarch (Table S2). Chain-length distributions (CLDs) of amylopectin in nanostarch (Table S3). Integration of ^{1}H NMR peaks of native starch and nanostarch (Table S4). General XPS spectra of native starch and SNS samples (Figure S2). Elemental surface ratio of native starch and nanostarch (Table S5). Analyses of C 1s and O 1s of native starch and nanostarch samples (Table S6). Characterization of microfluidization starch nanosphere (×1, 100 MPa) without nanoprecipitation. (Figure S3). (PDF)

AUTHOR INFORMATION

Corresponding Author

Enbo Xu − *College of Biosystems Engineering and Food Science, National Engineering Laboratory of Intelligent Food Technology and Equipment, State Key Laboratory of Fluid Power and Mechatronic Systems, Zhejiang Key Laboratory for Agro-Food Processing, Fuli Institute of Food Science, Zhejiang University, Hangzhou 310058, China; Innovation Center of Yangtze River Delta, Zhejiang University, Jiaxing 314102, China;* orcid.org/0000-0003-3869-9008; Email: enbo_xu@163.com, enboxu@zju.edu.cn

https://doi.org/10.1021/acssuschemeng.3c00575
ACS Sustainable Chem. Eng. 2023, 11, 7475−7488

Authors

Siyu Yao − *College of Biosystems Engineering and Food Science, National Engineering Laboratory of Intelligent Food Technology and Equipment, State Key Laboratory of Fluid Power and Mechatronic Systems, Zhejiang Key Laboratory for Agro-Food Processing, Fuli Institute of Food Science, Zhejiang University, Hangzhou 310058, China;* orcid.org/0000-0002-5391-889X

Shuohan Ma − *College of Biosystems Engineering and Food Science, National Engineering Laboratory of Intelligent Food Technology and Equipment, State Key Laboratory of Fluid Power and Mechatronic Systems, Zhejiang Key Laboratory for Agro-Food Processing, Fuli Institute of Food Science, Zhejiang University, Hangzhou 310058, China;* orcid.org/0000-0002-5280-3791

Qingqing Zhu − *College of Biosystems Engineering and Food Science, National Engineering Laboratory of Intelligent Food Technology and Equipment, State Key Laboratory of Fluid Power and Mechatronic Systems, Zhejiang Key Laboratory for Agro-Food Processing, Fuli Institute of Food Science, Zhejiang University, Hangzhou 310058, China; Innovation Center of Yangtze River Delta, Zhejiang University, Jiaxing 314102, China*

Yu Qin − *College of Biosystems Engineering and Food Science, National Engineering Laboratory of Intelligent Food Technology and Equipment, State Key Laboratory of Fluid Power and Mechatronic Systems, Zhejiang Key Laboratory for Agro-Food Processing, Fuli Institute of Food Science, Zhejiang University, Hangzhou 310058, China*

Wei-ying Ngah − *College of Biosystems Engineering and Food Science, National Engineering Laboratory of Intelligent Food Technology and Equipment, State Key Laboratory of Fluid Power and Mechatronic Systems, Zhejiang Key Laboratory for Agro-Food Processing, Fuli Institute of Food Science, Zhejiang University, Hangzhou 310058, China*

Youming Zuo − *Institute of Nuclear Agricultural Sciences, Zhejiang University, Hangzhou 310058, China*

Yu Liu − *College of Life Sciences, Zhejiang University, Hangzhou 310058, China*

Ximing Zhang − *College of Biosystems Engineering and Food Science, National Engineering Laboratory of Intelligent Food Technology and Equipment, State Key Laboratory of Fluid Power and Mechatronic Systems, Zhejiang Key Laboratory for Agro-Food Processing, Fuli Institute of Food Science, Zhejiang University, Hangzhou 310058, China;* orcid.org/0000-0002-4889-8791

Jinhu Tian − *College of Biosystems Engineering and Food Science, National Engineering Laboratory of Intelligent Food Technology and Equipment, State Key Laboratory of Fluid Power and Mechatronic Systems, Zhejiang Key Laboratory for Agro-Food Processing, Fuli Institute of Food Science, Zhejiang University, Hangzhou 310058, China; Innovation Center of Yangtze River Delta, Zhejiang University, Jiaxing 314102, China*

Xiangli Kong − *Institute of Nuclear Agricultural Sciences, Zhejiang University, Hangzhou 310058, China*

Donghong Liu − *College of Biosystems Engineering and Food Science, National Engineering Laboratory of Intelligent Food Technology and Equipment, State Key Laboratory of Fluid Power and Mechatronic Systems, Zhejiang Key Laboratory for Agro-Food Processing, Fuli Institute of Food Science, Zhejiang University, Hangzhou 310058, China; Innovation Center of Yangtze River Delta, Zhejiang University, Jiaxing 314102, China*

Complete contact information is available at: https://pubs.acs.org/10.1021/acssuschemeng.3c00575

Author Contributions

Writing—original draft, Siyu Yao and Enbo Xu. Data curation and investigation, Shuohan Ma, Qingqing Zhu, Yu Qin, and Wei-ying Ngah.Computational analysis and validation, Youming Zuo and Yu Liu. Review, editing, conceptualization and supervision, Ximing Zhang, Jinhu Tian, Xiangli Kong, Donghong Liu, and Enbo Xu. Funding acquisition, Enbo Xu. All authors have read and agreed to the published version of the manuscript.

Funding

This work was supported by the Natural Science Foundation of China (32272464), National Key Research and Development Program of China (2022YFF1101800), Young Elite Scientists Sponsorship Program by CAST (2022QNRC001), and Starry Night Science Fund of Zhejiang University Shanghai Institute for Advanced Study (SN-ZJU-SIAS-004). We also thank the Project Supported by Scientific Research Fund of Zhejiang Provincial Education Department (Y202250819).

Notes

The authors declare no competing financial interest.

■ ABBREVIATIONS

DHPM, dynamic high-pressure microfluidization; SNS, starch nanosphere; DS, degree of substitution; CLD, chain-length distribution; ISI, iodine staining index; AC, amylose content; BD, branching degree; DO, degree of order; DD, degree of double helices; DMSO, dimethyl sulfoxide; DLS, dynamic light scattering; SEM, scanning electron microscope; TEM, transmission electron microscopy; XRD, X-ray powder diffraction; FTIR, Fourier transform infrared spectrometer; XPS, X-ray photoelectron spectrum; ^{1}H NMR, ^{1}H-Nuclear magnetic resonance; ^{13}C NMR, ^{13}C-Nuclear magnetic resonance; SEC, size-exclusion chromatography; HPAEC, high-performance anion-exchange chromatography

■ REFERENCES

(1) Guo, Z.; Zeng, S.; Lu, X.; Zhou, M.; Zheng, M.; Zheng, B. Structural and physicochemical properties of lotus seed starch treated with ultra-high pressure. *Food Chem.* **2015**, *186*, 223−230.

(2) Lu, H.; Tian, Y. Nanostarch: preparation, modification, and application in Pickering emulsions. *J. Agric. Food Chem.* **2021**, *69* (25), 6929−6942.

(3) Poonguzhali, R.; Khaleel Basha, S.; Sugantha Kumari, V. Fabrication of asymmetric nanostarch reinforced Chitosan/PVP membrane and its evaluation as an antibacterial patch for in vivo wound healing application. *Int. J. Biol. Macromol.* **2018**, *114*, 204−213.

(4) Poonguzhali, R.; Basha, S. K.; Kumari, V. S. Nanostarch Reinforced with Chitosan/Poly (vinyl pyrrolidone) Blend for In Vitro Wound Healing Application. *Polym.-Plast. Technol. Eng.* **2018**, *57* (14), 1400−1410.

(5) Bel Haaj, S.; Thielemans, W.; Magnin, A.; Boufi, S. Starch nanocrystals and starch nanoparticles from waxy maize as nanoreinforcement: A comparative study. *Carbohydr. Polym.* **2016**, *143*, 310−317.

(6) Dukare, A. S.; Arputharaj, A.; Bharimalla, A. K.; Saxena, S.; Vigneshwaran, N. Nanostarch production by enzymatic hydrolysis of

cereal and tuber starches. *Carbohydr. Polym. Technol. and Applications* **2021**, *2*, 100121.
(7) Wang, B.; Lin, X.; Zheng, Y.; Zeng, M.; Huang, M.; Guo, Z. Effect of homogenization-pressure-assisted enzymatic hydrolysis on the structural and physicochemical properties of lotus-seed starch nanoparticles. *Int. J. Biol. Macromol.* **2021**, *167*, 1579−1586.
(8) Domingues, C.; Santos, A.; Alvarez-Lorenzo, C.; Concheiro, A.; Jarak, I.; Veiga, F.; Barbosa, I.; Dourado, M.; Figueiras, A. Where Is Nano Today and Where Is It Headed? A Review of Nanomedicine and the Dilemma of Nanotoxicology. *ACS Nano* **2022**, *16* (7), 9994−10041.
(9) Lin, Q.; Liang, R.; Zhong, F.; Ye, A.; Hemar, Y.; Yang, Z.; Singh, H. Self-Assembled Micelles Based on OSA-Modified Starches for Enhancing Solubility of β-Carotene: Effect of Starch Macromolecular Architecture. *J. Agric. Food Chem.* **2019**, *67* (23), 6614−6624.
(10) Qiu, C.; Wang, C.; Gong, C.; McClements, D. J.; Jin, Z.; Wang, J. Advances in research on preparation, characterization, interaction with proteins, digestion and delivery systems of starch-based nanoparticles. *Int. J. Biol. Macromol.* **2020**, *152*, 117−125.
(11) Dufresne, A.; Cavaille, J.-Y.; Helbert, W. New nanocomposite materials: Microcrystalline starch reinforced thermoplastic. *Macromolecules* **1996**, *29* (23), 7624−7626.
(12) Kaur, J.; Kaur, G.; Sharma, S.; Jeet, K. Cereal Starch Nanoparticles- A P rospectiveFood Additive: A Review. *Crit. Rev. Food Sci. Nutr.* **2018**, *58*, 1097−1107.
(13) Kumari, S.; Yadav, B. S.; Yadav, R. B. Synthesis and modification approaches for starch nanoparticles for their emerging food industrial applications: A review. *F ood Res. Int.* **2020**, *128*, 108765.
(14) Campelo, P .H.; Sant'Ana, A. S.; P edrosa Silva Clerici, M. T. Starch nanoparticles: production methods, structure, and properties for food applications. *Curr. Opin. F ood Sci.* **2020**, *33*, 136−140.
(15) Qiu, C.; Hu, Y.; Jin, Z.; McClements, D. J.; Qin, Y.; Xu, X.; Wang, J. A review of green techniques for the synthesis of size-controlled starch-based nanoparticles and their applications as nanodelivery systems. *Trends F ood Sci. Technol.* **2019**, *92*, 138−151.
(16) Ruan, S.; Tang, J.; Qin, Y.; Wang, J.; Yan, T.; Zhou, J.; Gao, D.; Xu, E.; Liu, D. Mechanical force-induced dispersion of starch nanoparticles and nanoemulsion: Size control, dispersion behaviour, and emulsified stability. *Carbohydr. Polym.* **2022**, *275*, 118711.
(17) Mahmoudi Najafi, S. H.; Baghaie, M.; Ashori, A. Preparation and characterization of acetylated starch nanoparticles as drug carrier: Active Ingredient as a model. *Int. J. Biol. Macromol.* **2016**, *87*, 48−54.
(18) Wu, X.; Zhao, L.; Fang, F.; Guo, Y.; Liang, W.; Ma, Y.; Wang, K. P rogressin understanding the interaction between bioactive components of soybean and gut microbiota. *Food Sci.* **2021**, *42* (13), 265−272.
(19) Ozturk, O. K.; Turasan, H. Applications of microfluidization in emulsion-based systems, nanoparticle formation, and beverages. *Trends F ood Sci. Technol.* **2021**, *116*, 609−625.
(20) Zhu, F. Structure and physicochemical properties of starch affected by dynamic pressure treatments: A review. *Trends F ood Sci. Technol.* **2021**, *116*, 639−654.
(21) Chen, L.; Dai, Y.; Hou, H.; Wang, W.; Ding, X.; Zhang, H.; Li, X.; Dong, H. Effect of high pressure microfluidization on the morphology, structure and rheology of sweet potato starch. *Food Hydrocoll.* **2021**, *115*, 106606.
(22) He, X.-h.; Luo, S.-j.; Chen, M.-s.; Xia, W.; Chen, J.; Liu, C.-m. Effect of industry-scale microfluidization on structural and physicochemical properties of potato starch. *Innov. F ood Sci. Emerg. Technol.* **2020**, *60*, 102278.
(23) Bitik, A.; Sumnu, G.; Oztop, M. Physicochemical and Structural Characterization of Microfluidized and Sonicated Legume Starches. *F oodBioprocess Technol.* **2019**, *12* (7), 1144−1156.
(24) Che, L.-M.; Wang, L.-J.; Li, D.; Bhandari, B.; Ozkan, N.; Chen, L. D.; Mao, Z.-H. Starch pastes thinning during high-pressure homogenization. *Carbohydr. Polym.* **2009**, *75* (1), 32−38.
(25) Tu, Z.; Yin, Y.; Wang, H.; Liu, G.; Chen, L.; Zhang, P.; Kou, Y.; Zhang, L. Effect of dynamic high-pressure microfluidization on theP morphology characteristics and physicochemical properties of maize amylose. *Starch-Starke* **2013**, *65* (5−6), 390−397.
(26) Kasemwong, K.; Ruktanonchai, U. R.; Srinuanchai, W.; Itthisoponkul, T.; Sriroth, K. Effect of high-pressure microfluidization on the structure of cassava starch granule. *Starch-Starke* **2011**, *63* (3), 160−170.
(27) Joye, I. J.; McClements, D. J. Production of nanoparticles by anti-solvent precipitation for use in food systems. *Trends Food Sci. Technol.* **2013**, *34* (2), 109−123.
(28) Tan, Y.; Xu, K.; Li, L.; Liu, C.; Song, C.; Wang, P. Fabrication of Size-Controlled Starch-Based Nanospheres by Nanoprecipitation. *ACS Appl. Mater. Interfaces* **2009**, *1* (4), 956.
(29) Lebouille, J.G.J.L.; Stepanyan, R.; Slot, J.J.M.; Cohen Stuart, M.A.; Tuinier, R. Nanoprecipitation of polymers in a bad solvent. *Colloid Surf. A-Physicochem. Eng. Asp.* **2014**, *460* (9), 225−235.
(30) Takeda, Y.; Shibahara, S.; Hanashiro, I. Examination of the structure of amylopectin molecules by fluorescent labeling. *Carbohydr. Res.* **2003**, *338* (5), 471−475.
(31) Fu, Z.; Luo, S.-J.; BeMiller, J. N.; Liu, W.; Liu, C.-M. Effect of high-speed jet on flow behavior, retrogradation, and molecular weight of rice starch. *Carbohydr. Polym.* **2015**, *133*, 61−66.
(32) Wei, B.; Cai, C.; Xu, B.; Jin, Z.; Tian, Y. Disruption and molecule degradation of waxy maize starch granules during high pressure homogenization process. *Food Chem.* **2018**, *240*, 165−173.
(33) Tang, J.; Zhou, J.; Zhou, X.; Li, D.; Wu, Z.; Tian, J.; Xu, E.; Liu, D. Rearranged supramolecular structure of resistant starch with polymorphic microcrystals prepared in high-solid enzymatic system. *Food Hydrocoll.* **2022**, *124*, 107215.
(34) Chen, L.; Xiong, Z.; Xiong, H.; Din, Z.-u. Investigating the structure and self-assembly behavior of starch-g-VAc in starch-based adhesive by combining NMR analysis and multi-scale simulation. *Carbohydr. Polym.* **2020**, *246*, 116655.
(35) Chang, R.; Xiong, L.; Li, M.; Liu, J.; Wang, Y.; Chen, H.; Sun, Q. Fractionation of debranched starch with different molecular weights via edible alcohol precipitation. *Food Hydrocoll.* **2018**, *83*, 430−437.
(36) Kong, X.; Chen, Y.; Zhu, P.; Sui, Z.; Corke, H.; Bao, J. Relationships among Genetic, Structural, and Functional Properties of Rice Starch. *J. Agric. Food Chem.* **2015**, *63* (27), 6241−6248.
(37) You, Q. The effect of dynamic high-pressure microfluidization on the structure and physicochemical properties of lotus seed starch. Master's Thesis, Fujian Agriculture and Forestry University: Fujian, China, 2020.
(38) Liu, P.; Liu, Z.; Kennedy, J. F. The study of starch nano-unit chains in the gelatinization process. *Carbohydr. Polym.* **2007**, *68* (2), 360−366.
(39) Wang, Z.; Zhang, Y.; Liu, W.; Gu, Z.; Cheng, L.; Li, Z. Effects of Gelatinization Pretreatment on the Performance of Starch-Based Wood Adhesive. *Food Sci. Biotechnol.* **2012**, *31* (8), 844−848.
(40) Zhang, Z.; Zhao, S.; Xiong, S. Morphology and physicochemical properties of mechanically activated rice starch. *Carbohydr. Polym.* **2010**, *79* (2), 341−348.
(41) Bolm, C.; Hernández, J. G. Mechanochemistry of Gaseous Reactants. *Angew. Chem., Int. Ed.* **2019**, *58* (11), 3285−3299.
(42) Mucsi, G. A review on mechanical activation and mechanical alloying in stirred media mill. *Chem. Eng. Res. Des.* **2019**, *148*, 460−474.
(43) You, Q.; Zeng, H.; Chen, P.; Lin, Y.; Zheng, B.; Zhang, Y. Structural and physicochemical properties of modified starch by dynamic high pressure microfluidization. *Food Ferment. Ind.* **2019**, *45* (19), 307−315.
(44) Klaochanpong, N.; Puttanlek, C.; Rungsardthong, V.; Puncha-Arnon, S.; Uttapap, D. Physicochemical and structural properties of debranched waxy rice, waxy corn and waxy potato starches. *Food Hydrocoll.* **2015**, *45*, 218−226.
(45) Apostolidis, E.; Mandala, I. Modification of resistant starch nanoparticles using high-pressure homogenization treatment. *Food Hydrocoll.* **2020**, *103*, 105677.

https://doi.org/10.1021/acssuschemeng.3c00575
ACS Sustainable Chem. Eng. 2023, 11, 7475−7488

(46) Hanashiro, I.; Abe, J. I.; Hizukuri, S. A periodic distribution of the chain length of amylopectin as revealed by high-performance anion-exchange chromatography. *Carbohydr. Res.* **1996**, *283* (none), 151−159.
(47) Chen, P. Morphology and gelatinization of corn starches with different amylose/amylopectin content under shearless and shear conditions. Ph.D. Thesis, South China University of Technology: Guangdong, China, 2010.
(48) Wei, B.; Cai, C.; Jin, Z.; Tian, Y. High-pressure homogenization induced degradation of amylopectin in a gelatinized state. *Starch-Starke* **2016**, *68* (7−8), 734−741.
(49) Xu, E.; Wu, Z.; Long, J.; Jiao, A.; Jin, Z. Porous Starch-Based Material Prepared by Bioextrusion in the Presence of Zinc and Amylase−Magnesium Complex. *ACS Sustain. Chem. Eng.* **2018**, *6* (8), 9572−9578.
(50) Qiu, C.; Yang, J.; Ge, S.; Chang, R.; Xiong, L.; Sun, Q. Preparation and characterization of size-controlled starch nanoparticles based on short linear chains from debranched waxy corn starch. *LWT* **2016**, *74*, 303−310.
(51) Fan, H.; Chen, Z.; Xu, L.; Wen, Y.; Li, H.; Wang, J.; Sun, B. Both alkyl chain length and V-amylose structure affect the structural and digestive stability of amylose-alkylresorcinols inclusion complexes. *Carbohydr. Polym.* **2022**, *292*, 119567.
(52) Ning, Y.; Cui, B.; Yuan, C.; Zou, Y.; Liu, W.; Pan, Y. Effects of konjac glucomannan on the rheological, microstructure and digestibility properties of debranched corn starch. *Food Hydrocoll.* **2020**, *100*, 105342.
(53) van Soest, J. J.G.; Tournois, H.; de Wit, D.; Vliegenthart, J. F.G. Short-range structure in (partially) crystalline potato starch determined with attenuated total reflectance Fourier-transform IR spectroscopy. *Carbohydr. Res.* **1995**, *279*, 201−214.
(54) Sun, Q.; Li, G.; Dai, L.; Ji, N.; Xiong, L. Green preparation and characterisation of waxy maize starch nanoparticles through enzymolysis and recrystallisation. *Food Chem.* **2014**, *162*, 223−228.
(55) Lopez-Silva, M.; Bello-Perez, L. A.; Agama-Acevedo, E.; Alvarez-Ramirez, J. Effect of amylose content in morphological, functional and emulsification properties of OSA modified corn starch. *Food Hydrocoll.* **2019**, *97*, 105212.
(56) Kizil, R.; Irudayaraj, J.; Seetharaman, K. Characterization of Irradiated Starches by Using FT-Raman and FTIR Spectroscopy. *J. Agric. Food Chem.* **2002**, *50* (14), 3912−3918.
(57) Sevenou, O.; Hill, S. E.; Farhat, I. A.; Mitchell, J. R. Organisation of the external region of the starch granule as determined by infrared spectroscopy. *Int. J. Biol. Macromol.* **2002**, *31* (1), 79−85.
(58) Bie, P.; Pu, H.; Zhang, B.; Su, J.; Chen, L.; Li, X. Structural characteristics and rheological properties of plasma-treated starch. *Innov. Food Sci. Emerg. Technol.* **2016**, *34*, 196−204.
(59) Zeng, H.; Chen, P.; Chen, C.; Huang, C.; Lin, S.; Zheng, B.; Zhang, Y. Structural properties and prebiotic activities of fractionated lotus seed resistant starches. *Food Chem.* **2018**, *251*, 33−40.
(60) Yin, X.; Hu, Z.; Zheng, Y.; Chai, Z.; Kong, X.; Chen, S.; Ye, X.; Tian, J. Multi-scale structure characterization and in vivo digestion of parboiled rice. *Food Chem.* **2023**, *402*, 134502.
(61) Gidley, M. J.; Bociek, S. M. Molecular organization in starches: a carbon 13 CP/MAS NMR study. *J. Am. Chem. Soc.* **1985**, *107* (24), 7040−7044.
(62) Mo, Z. S. *Crystallization and Structure of Macromolecules*; Science Press, 2017.
(63) Cheetham, N. W. H.; Tao, L. Solid state NMR studies on the structural and conformational properties of natural maize starches. *Carbohydr. Res.* **1998**, *36* (4), 285−292.
(64) Veregin, R. P.; Fyfe, C. A.; Marchessault, R. H. Investigation of the crystalline ″V″ amylose complexes by high-resolution carbon-13 CP/MAS NMR spectroscopy. *Macromolecules* **1987**, *20* (12), 3007−3012.
(65) Zhu, F. NMR spectroscopy of starch systems. *Food Hydrocoll.* **2017**, *63*, 611−624.
(66) Shi, L.; Zhou, J.; Guo, J.; Gladden, I.; Kong, L. Starch inclusion complex for the encapsulation and controlled release of bioactive guest compounds. *Carbohydr. Polym.* **2021**, *274*, 118596.
(67) Putseys, J. A.; Lamberts, L.; Delcour, J. A. Amylose-inclusion complexes: Formation, identity and physico-chemical properties. *J. Cereal Sci.* **2010**, *51* (3), 238−247.
(68) Nicolas, J.; Mura, S.; Brambilla, D.; Mackiewicz, N.; Couvreur, P. Design, functionalization strategies and biomedical applications of targeted biodegradable/biocompatible polymer-based nanocarriers for drug delivery. *Chem. Soc. Rev.* **2013**, *42*, 1147−1235.
(69) Lin, Q.; Liu, Y.; Zhou, L.; Ji, N.; Xiong, L.; Sun, Q. Green preparation of debranched starch nanoparticles with different crystalline structures by electrostatic spraying. *Food Hydrocoll.* **2022**, *127*, 107513.

https://doi.org/10.1021/acssuschemeng.3c00575
ACS Sustainable Chem. Eng. 2023, 11, 7475−7488